Biosynthesis of silver and gold nanoparticles using *Annona squamosa* seed extract: Insights into antibacterial and anticancer activities

FIRLI RAHMAH PRIMULA DEWI[1,2], AULIA UMI ROHMATIKA[1,3], ALMANDO GERALDI[1,4,5], A'LIYATUR ROSYIDAH[6], ARNIZA KHAIRANI MOHD JAMIL[7], TURAN DEMIRCAN[8], VERSA RACHMANIA HAJAR[1] and AMELIORA CLAREISTA ELFENTIANA[1]

[1]Department of Biology, Faculty of Science and Technology, Universitas Airlangga, Surabaya, East Java 60115, Indonesia; [2]Research Center for Stem Cells Development, Universitas Airlangga, Surabaya, East Java 60115, Indonesia; [3]Faculty of Medicine, Universitas Pembangunan Nasional 'Veteran' Jawa Timur, Surabaya, East Java 60294, Indonesia; [4]University CoE-Research Center for Bio-Molecule Engineering, Universitas Airlangga, Surabaya, East Java 60115, Indonesia; [5]Institute of Life Science, Technology and Engineering (LIHTR), Universitas Airlangga, Surabaya, East Java 60115, Indonesia; [6]Research Center for Vaccine and Drugs, Research Organization for Health, National Research and Innovation Agency (BRIN), Bogor 16911, Indonesia; [7]Department of Chemistry, Faculty of Science, Universiti Malaya, Kuala Lumpur 50603, Malaysia; [8]Department of Medical Biology, School of Medicine, İzmir Bakırçay University, İzmir 35665, Turkey

Received September 16, 2025; Accepted June 16, 2026

DOI: 10.3892/br.2026.2177

Abstract. This study reports on the green synthesis of silver nanoparticles (AgNPs) and gold nanoparticles (AuNPs) using *Annona squamosa* seed extract and the evaluation of their antibacterial and anticancer activities. The synthesized NPs were characterized by UV-Vis spectroscopy, transmission electron microscopy, particle size and size distribution analysis, X-ray diffraction, Fourier-Transform Infrared Spectroscopy and Inductively Coupled Plasma-Optical Emission Spectrometry. Characterization results confirmed the successful synthesis of spherical, crystalline NPs with mean hydrodynamic diameters of AgNPs and AuNPs determined as 40.60 and 72.65 nm, respectively. Antibacterial activity was assessed against *Staphylococcus aureus* and *Escherichia coli*, while anticancer activity was evaluated using MCF-7 breast cancer cells and 293 cells. AgNPs exhibited significant antibacterial activity against both bacterial species, showing bacteriostatic activity against *S. aureus* and bactericidal activity against *E. coli*. By contrast, AuNPs showed no detectable antibacterial effect. AgNPs also demonstrated selective anticancer activity, inhibiting MCF-7 cell proliferation in a dose- and time-dependent manner with IC_{50} values of 106.704 and 79.519 μg/ml after 48 and 72 h of treatment, respectively, while exhibiting minimal toxicity toward 293 cells. Furthermore, AgNPs modulated the expression of several cancer-related genes, suppressed oncogenic markers and induced apoptosis through activation of p53-associated pathways, as evidenced by increased apoptotic cell populations and an elevated BAX/BCL2 ratio. Conversely, AuNPs displayed limited biological activity under the tested conditions. These findings highlight the potential of *A. squamosa*-mediated AgNPs as promising antibacterial and selective anticancer agents for future biomedical applications.

Correspondence to: Dr Firli Rahmah Primula Dewi, Department of Biology, Faculty of Science and Technology, Universitas Airlangga, Jl. Dr. Ir. H. Soekarno 123, Mulyorejo, Surabaya, East Java 60115, Indonesia
E-mail: firli.rahmah@fst.unair.ac.id

Key words: breast cancer, antibacterial, green synthesis, metal nanoparticles, *A. squamosa* seeds extract

Introduction

The emerging field of bionanotechnology-where nanotechnology meets biotechnology-offers exciting new possibilities for various applications (1). Recent advances have driven major breakthroughs across different technological domains. In particular, nanoparticles (NPs)-tiny engineered materials between 1-100 nanometers in size-have captured researchers' attention due to their unique properties (2-4). Metal NPs especially stand out because they are highly stable, easy to modify chemically and effective at enhancing permeability (5).

The demand for NPs is rapidly increasing across various sectors due to their versatile applications (6). These applications span multiple industries, including biomedical fields, energy sectors and chemistry (7,8). Silver (Ag) and gold (Au) NPs are particularly promising for biomedical uses. AuNPs, for example, help detect and kill cancer cells. They can effectively heat and destroy cancer cells after being absorbed, even triggering cell death in lymphocytic leukemia (9,10). Studies have also shown that AuNPs derived from *Suaeda monoica* and *Nerium oleander* leaves extract have powerful antioxidant

effects (11,12). AgNPs are similarly versatile-they're used in everything from biological labeling to antibacterial treatments, sensors, electrodes and integrated circuits. They've proven especially effective against various disease-causing pathogens (13).

AgNPs and AuNPs can be synthesized using chemical, physical and biological methods (14,15). Successful NP synthesis relies on selecting eco-friendly solvents, efficient reducing agents and non-toxic stabilizing materials. Among the various synthesis techniques, physical, chemical and biosynthetic methods are commonly used. While traditional chemical approaches work, they often involve harsh chemicals and can be costly (16). By contrast, biosynthetic methods using plants and microorganisms offer a gentler approach that's especially valuable for medical applications (17-19). Plants are particularly useful in this process because they contain natural compounds such as flavonoids and saponins that can both reduce metal salts and stabilize the resulting NPs (20). This green approach is gaining popularity because it's cost-effective, environmentally friendly and produces stable, high-quality NPs without harmful contamination (13,21).

The *Annona squamosa* (*A. squamosa*) plant, commonly known as custard apple, has proven particularly valuable in this field. Several studies have utilized different parts of the *A. squamosa* plant, including leaves (22-24), seeds (25-27), fruits (23,28) and peel extract (29) for the biosynthesis of AgNPs and AuNPs, and have examined their antibacterial, anticancer, antioxidant, anti-arthritic and larvicidal activities (28-30). Of note, while numerous parts of the plant have been studied, to the best of our knowledge, no one has yet explored using the seeds to make AuNPs or tested seed-derived AgNPs against cancer and non-cancerous cells. The present study fills this gap by creating both silver and gold nanoparticles from *A. squamosa* seeds and testing their effectiveness against bacteria, breast cancer cells (MCF-7) and normal/non-carcinogenic cells (293 cells).

Materials and methods

Synthesis of AgNPs. A. squamosa seed extract was procured from Anhui Minmetals Development Ltd. To prepare the *A. squamosa* seed extract solution, 0.3 g of the powder was dissolved in 100 ml of ddH_2O. For synthesizing AgNPs, 33 ml of *A. squamosa* seeds extract solution was added with 33 ml of a 0.1 M of silver nitrate ($AgNO_3$). The pH of the mixture was adjusted to 7.0 and the mixture was heated at 60˚C for 5 min and incubated under the exclusion of light for 24 h. The successful formation of of AgNPs was marked by a color change from light to dark brown.

Synthesis of AuNPs. AuNP synthesis begins with making a gold ion solution by mixing 100 mg of $HAuCl_4$ (Smart Lab, Indonesia) in 100 ml of ddH_2O. To produce AuNPs, 100 ml of $HAuCl_4$ solution was combined with 100 ml of *A. squamosa* seed extract solution. The mixture was then incubated under the exclusion of light for 24 h. The appearance of AuNPs was marked by a color change from light brown to purple.

Characterization of AgNPs and AuNPs. The synthesis of AgNPs and AuNPs was independently repeated at least three times to assess reproducibility. The consistency and formation of the NPs were confirmed by UV-vis spectrophotometry and particle size analysis (PSA). The presence of AgNPs and AuNPs was initially verified based on their characteristic surface plasmon resonance absorption bands. Functional groups associated with the biomolecules responsible for the reduction and stabilization processes were analyzed using a Spectrum 100 FT-IR spectrometer (PerkinElmer, Inc.) within the wavenumber range of 4,000-400/cm. Furthermore, PSA was employed to determine the hydrodynamic size distribution of the NPs in the liquid phase. This method was commenced with an analysis of refractive index and viscosity in the test samples and was crucial for understanding NP properties such as chemical receptivity, stability and biocompatibility. Subsequently, 2 ml of sample was introduced into a PSA analysis cuvette, where a laser beam was emitted into the sample and the intensity of the reflected light was measured to ascertain particle size and distribution (30). Additionally, NP size distribution was measured using a ViewSizer 3000 NP Size Analyzer (Horiba Scientific). Measurements were performed using blue (B, 445 nm), green (G, 520 nm) and red (R, 635 nm) lasers with pulse durations of 15 msec for each channel (B/G/R: 15/15/15 msec). Transmission electron microscopy (TEM) was used for morphology analysis of the NPs (FEI Tecnai G2 F20 X-TWIN; Thermo Fisher Scientific, Inc.). A small aliquot of NPs was deposited onto a copper grid, allowed to dry at room temperature and subsequently analyzed by TEM. TEM images were obtained from the electron beam transmitted through the thin NP sample. The crystalline properties of the biosynthesized NPs were characterized using a PANalytical Empyrean X-ray Diffractometer (EA Almelo). Before X-ray diffraction (XRD) analysis, the NPs were freeze-dried with a Lyovapor L-200 (Buchi) at temperatures between -55 and -57˚C under a pressure of 2 mbar for 24-48 h. The freeze-dried samples were then subjected to XRD analysis using Cu Kα radiation, with diffraction data collected over a 2θ range of 5˚-80˚.

Metal content evaluation of AgNPs. The Ag content of the NPs was quantified using an Agilent 5100 Inductively Coupled Plasma-Optical Emission Spectrometer (ICP-OES; Agilent Technologies, Inc.). Prior to analysis, the AgNPs samples were digested in an acidic medium prepared from ultrapure water containing 12% (v/v) hydrochloric acid (37%) and 4% (v/v) nitric acid (65%). The digestion process was carried out at 95±2˚C for 2 h, after which the solution volume was brought to 50 ml using the same acid mixture. The concentration of Ag in the NPs was determined according to the following equation according to the 2018 study by Shahid *et al* (31):

$$Content\ (\mu g/g) = \frac{Cs}{W} x\ V,$$

where Cs represents the Ag concentration measured in the digested solution by ICP-OES (Agilent 5100; Agilent Technologies, Inc.), W is the final volume of the digestion solution (ml) and V denotes the mass of the dried sample used for analysis (0.025 g).

Sterility evaluation of NPs. Sterile blank discs injected with 20 μl of AgNPs and AuNPs at a concentration of 100 mg/ml were placed onto sterile Mueller-Hinton Agar (MHA) plates media (Sisco Research Laboratories). Sterile blank discs injected with 20 μl of *S. aureus* and *E. coli* culture (10^8 CFU/ml)

were used as a positive control, while sterile nuclease-free water (Promega Corp.) served as a negative control. The plates were then incubated for 24 h at 37˚C, after which bacterial growth was observed.

Inoculum preparation of S. aureus and E. coli. *S. aureus* [American Type Culture Collection (ATCC) 25923] and *E. coli* (ATCC 25922) were obtained from the Applied Microbiology Laboratory at the University-CoE Research Center for Biomolecule Engineering, Universitas Airlangga. To prepare an overnight culture, a single colony of each strain was inoculated into Mueller-Hinton Broth (MHB) (Sisco Research Laboratories) and incubated at 37˚C while shaking at 150 rpm for 24 h. Following this incubation, 60 μl of each overnight culture was transferred into 3 ml of sterile MHB and cultured at 37˚C while shaking at 150 rpm until the optical density (OD) at 600 nm (OD_{600}) reached 0.1. The OD was measured using a NanoPhotometer NP80 (Implen GmbH) (32).

Antibacterial evaluation of AgNPs and AuNPs. A modified method based on the Clinical and Laboratory Standards Institute document M02-ed14 (32) was used to assess the antibacterial activity of the *A. squamosa* seeds extract, AuNPs and AgNPs. Each assay was performed in triplicate. Using a cotton swab, 100 μl of cultured test bacteria were spread onto MHA plates. A total of 20 μl of an antibiotic or NPs at different concentrations were applied to sterile blank discs, which were then placed on the agar media inoculated with the test microbes. Gentamicin (40 mg/ml) was used as a positive control. A caliper was used to measure the clear zone resulting from the inhibition of microbial growth.

The minimum inhibitory concentration (MIC) test was conducted in triplicate by adding different concentrations of the AgNPs from 50 to 0.098 mg/ml to MHB media inoculated with 10^5 colony-forming units/ml *E. coli* or *S. aureus* in a 96-well microplate. The OD at 600 nm was measured using a microplate reader before and after incubation at 37˚C for 24 h. The MIC or the lowest concentration of the AgNPs that prevents bacterial growth is observed when there is no increase in OD_{600} value after 24 h of incubation. Meanwhile, the minimum bactericidal concentration (MBC) was determined by spreading 100 μl of bacterial culture treated by AgNPs at the MIC concentration and two concentrations above it onto MHA plates. The MBC is the lowest concentration that inhibits any bacterial growth on the MHA plates.

Cell proliferation analysis and half-maximal inhibitory concentration (IC_{50}) determination. To evaluate the anticancer activity and selective cytotoxicity of the NPs, an MTT assay was performed. Human breast adenocarcinoma cells (MCF-7) [American Type Culture Collection (ATCC)] and 293 cells (ATCC) were cultured in Dulbecco's modified Eagle's medium (cat. no. D6429; Sigma-Aldrich; Merck KGaA) supplemented with 10% fetal bovine serum (FBS) (cat. no. F2442; Sigma-Aldrich; Merck KGaA) and 1% penicillin-streptomycin. 293 cells were used as a non-malignant control cell line because they are of human origin, exhibit stable growth characteristics and are widely employed in cytotoxicity studies to evaluate the selectivity and safety of anticancer agents (33). Cells were maintained at 37˚C in a humidified incubator containing 5% CO_2. For the cytotoxicity assay, cells were seeded into 96-well plates at a density of $5x10^3$ cells per well in 100 μl of complete medium and allowed to attach for 24 h. The culture medium was subsequently replaced with fresh medium containing NFW (control), doxorubicin (10 μg/ml; positive control), $AgNO_3$, AgNPs or AuNPs at concentrations of 12.5, 25, 50, 100 and 200 μg/ml. Cells were incubated with the treatments for 24, 48 and/or 72 h. Following the treatment period, 10 μl of MTT solution (5 mg/ml in PBS) was added to each well and incubated for 4 h at 37˚C. The resulting formazan crystals were dissolved by adding 100 μl of DMSO (Merck KGaA), followed by incubation in the dark until complete dissolution of the crystals. The absorbance was measured at 570 nm using a microplate reader.

The IC_{50} values were determined by plotting the percentage of cell viability against the logarithm of the NP concentration and fitting the data using nonlinear regression analysis (four-parameter logistic model) in GraphPad Prism 10 software (Dotmatics). The IC_{50} value was defined as the concentration required to reduce cell viability by 50% compared with the untreated control. All experiments were performed in triplicate.

Cell cycle and DNA content analysis. Cellular DNA content was assessed by staining with 4',6-diamidino-2-phenylindole (DAPI). In brief, cells were fixed in 4% paraformaldehyde and incubated with 1 μg/ml DAPI C001 (ABP Biosciences) for 20 min at room temperature in the dark. After staining, cells were washed three times with PBS and subjected to cell cycle analysis. Images were acquired using a Cell-Insight CX7 Pro High Content Screening (HCS) System (version 393216; Thermo Fisher Scientific, Inc.) with the assay parameters set to 'CellCycle.V4', an autofocus interval of 2, a PRIMEBSI 1.53 camera and a x20 objective lens. Image processing and cell cycle quantification were conducted using Thermo Scientific HCS Studio 5.0 Cell Analysis Software (Thermo Fisher Scientific, Inc.). Cell cycle phases were determined based on DNA content, where cells containing 2N DNA were classified as G1 phase, those with DNA content between 2N and 4N as S phase, and those with 4N DNA as G2/M phase.

RNA isolation and gene expression analysis. MCF-7 cells were cultured in 6-well plates and divided into three groups for a 48-h treatment period: A control group, a doxorubicin-treated group (10 μg/ml) and an AgNPs-treated group (100 μg/ml), with each group prepared in triplicate. The concentrations of AgNPs were determined close to the IC_{50} value. The RNA was extracted using the Total RNA Mini Kit (cat. no. RTD050; Geneaid). The cDNA was synthesized with ReverTra Ace qPCR RT Master Mix (cat. no. FSQ-201; Toyobo) according to the manufacturer's protocol, with 50 ng RNA contained in each sample. Quantitative PCR (qPCR) analysis was performed using Thunderbird Next SYBR qPCR Mix (cat. no. QPX-201; Toyobo) containing Tris (hydroxymethyl)aminomethane, magnesium sulfate, deoxyadenosine triphosphate, deoxycytidine triphosphate, deoxyguanosine triphosphate, deoxythymidine triphosphate, SYBR® Green I and DNA polymerase. Each qPCR reaction mixture consisted of 10 μl of THUNDERBIRD™ Next SYBR® qPCR Mix, 6 pmol each

Table I. Primer sequences for quantitative PCR analysis.

Genes	Primer sequence
MYC	F, 5'-GGAGGAACAAGAAGATGAGG-3'
	R, 5'-GTAGTTGTGCTGATGTGTGG-3'
CCND1	F, 5'-AACTACCTGGACCGCTTCCT-3'
	R, 5'-CCACTTGAGCTTGTTCACCA-3'
HER2	F, 5'-CCGAGGGCCGGTATACATTC-3'
	R, 5'-GCTTGCTGCACTTCTCACAC-3'
PTGS2 (encodes COX2)	F, 5'-CCGGGTACAATCGCACTTAT-3'
	R, 5'-GGCGCTCAGCCATACAG-3'
CTNND1	F, 5'-TCTGCCATAGCTGACCTCCT-3'
	R, 5'-GGAGTTCTGCTGTCCTCCTG-3'
TP53	F, 5'-TGC GTG TTT GTG CCT GTC CT-3'
	R, 5'-GTG CTC GCTTAGTGCTCCCT-3'
BBC3 (encodes PUMA)	F 5'-GACCTCAACGCACAGTACGAG-3'
	R, 5'-AGGAGTCCCATGATGAGATTGT-3'
BAX	F, 5'-TCTGACGGCAACTTCAACTG-3'
	R, 5'-TTGAGGAGTCTCACCCAACC-3'
BCL2	F, 5'-CAGCATGCGGCCTCTGTT-3'
	R, 5'-GGGCCAAACTGAGCAGAGTCT-3'
ACTB	F, 5'-CCACACTGTGCCCATCTACG-3'
	R, 5'-AGGATCTTCATGAGGTAGTCAGTCAG-3'
GAPDH	F, 5'-GTCAGTGGTGGACCTGACCT-3'
	R, 5'-AGGGGTCTACATGGCAACTG-3'

F, forward; R, reverse; *MYC*, c-Myc; *CCND1*, cyclin D1; *HER-2*, human epidermal growth factor receptor-2; *PTGS2*, prostaglandin-endoperoxide synthase 2*; COX-2*, cyclooxygenase-2; *CTNND1*, catenin delta-1; *TP53*, tumor protein P53; *BAX*, BCL2 associated X; *BBC3*/*PUMA*, BCL2 binding component 3; *BCL2*, B-cell lymphoma 2; *ACTB*, actin-β; *GAPDH*, glyceraldehyde 3-phosphate dehydrogenase.

of forward and reverse primers, 4 ng of cDNA template and nuclease-free water added to a final volume of 20 μl. The qPCR was performed with MyGo Pro Real-Time PCR System (IT-IS Life Science Ltd.) under the following cycling conditions: Predenaturation at 95˚C for 60 sec, followed by 40 cycles of denaturation at 95˚C for 5 sec and annealing/extension at 60˚C for 30 sec. The threshold value was determined automatically using MyGo Pro PCR Software version 3.5 (IT-IS Life Science Ltd.). Forward and reverse primers for c-Myc (MYC), cyclin D1 (CCND1), human epidermal growth factor receptor-2 (HER-2), cyclooxygenase-2 (COX-2), catenin delta-1 (CTNND1), tumor protein P53 (TP53), BCL2 associated X (BAX), BCL2 binding component 3 (BBC3/PUMA), BCL2, actin-b and GAPDH were referenced from previous studies (34-38). The primer sequences for the genes analyzed in this study are provided in Table I. Gene expression analysis was performed using the relative quantification method and the reliability of the qPCR results was verified through melting curve analysis. The fold change in mRNA expression was calculated using the ΔΔCq formula: $2^{-\Delta\Delta Cq}=2^{-[(Cqtarget-Cqreference)\ sample-(Cqtarget-Cqreference)\ calibrator]}$, where $Cq_{reference}$ refers to the housekeeping gene and calibrator indicates the control sample (39).

Flow cytometric analysis of apoptosis using Annexin V-FITC staining. Apoptosis analysis was performed on MCF-7 breast cancer cells using the Annexin V-FITC staining method followed by flow cytometric analysis. In brief, MCF-7 cells treated with AgNPs (100 μg/ml) and untreated control cells were harvested after the designated incubation period. Culture media containing floating cells were first collected into centrifuge tubes to preserve non-adherent apoptotic cells. The remaining adherent cells were washed with PBS and detached using TrypLE™ Express (cat. no. 12604013; Gibco; Thermo Fisher Scientific, Inc.). The enzymatic reaction was neutralized by adding complete culture medium supplemented with FBS. The collected cell suspension was centrifuged at 447 x g for 5 min at 4˚C and the resulting cell pellet was washed twice with cold PBS. Subsequently, the cell pellet was resuspended in 100 μl of 1X Annexin V Binding Buffer to obtain a final cell concentration of $1x10^5$-$1x10^6$ cells/ml. A total of 5 μl of Annexin V-FITC reagent was added to each sample, followed by gentle mixing and incubation for 15 min at room temperature (20-25˚C) in the dark. After incubation, 400 μl of 1X Annexin V Binding Buffer was added to each sample and the stained cells were transferred into fluorescence-assisted cell sorting tubes for analysis. Samples were analyzed immediately using a flow cytometer. The distribution of viable, early apoptotic, late apoptotic and necrotic cells was determined based on quadrant analysis of the resulting dot plots, which were generated according to Annexin V fluorescence intensity.

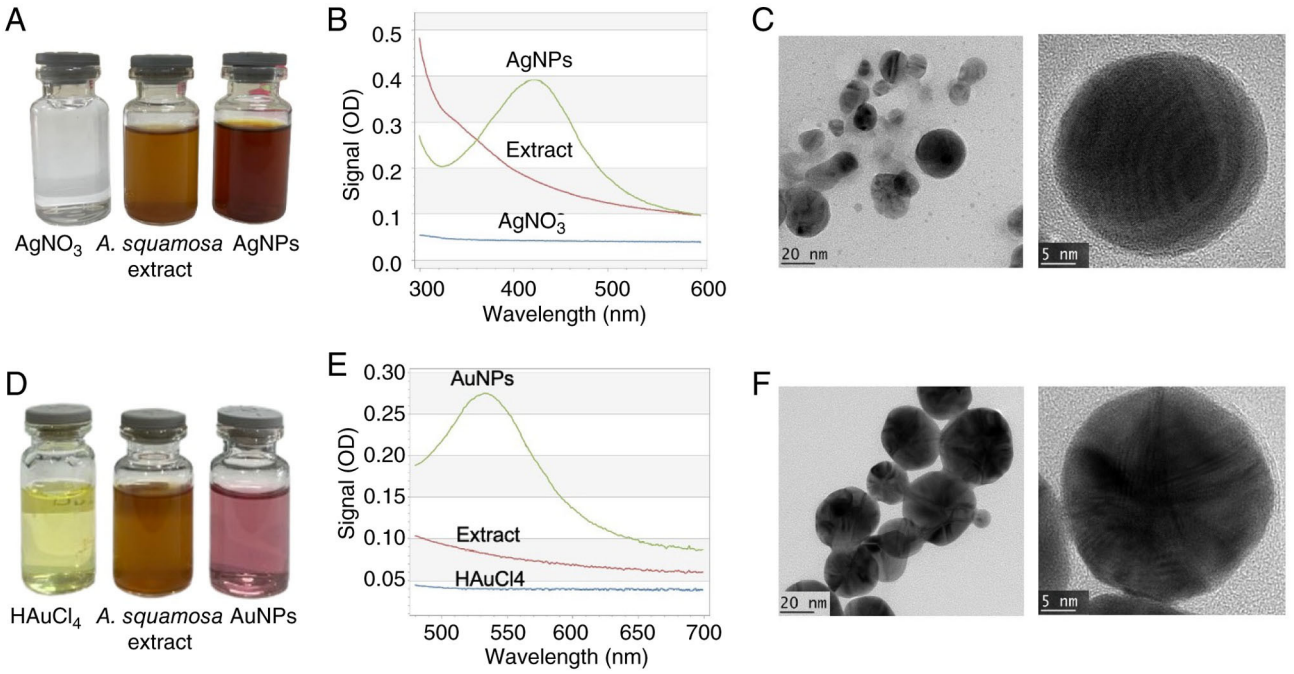

Figure 1. Synthesis of NPs using *A. squamosa* seeds extract and their characterization. (A) The observed color changes during the synthesis of AgNPs. (B) UV-Vis spectrophotometric analysis of the synthesized AgNPs. (C) TEM visualization of AgNPs synthesized using *A. squamosa* seed extract showing predominantly spherical NPs with crystalline lattice fringes (scale bars, 20 and 5 nm). (D) The color changes observed during the synthesis of AuNPs. (E) UV-Vis spectroscopic analysis of the synthesized AuNPs. (F) TEM visualization of AuNPs synthesized using *A. squamosa* seed extract exhibiting spherical to quasi-spherical morphology and highly ordered crystalline structures (scale bars, 20 and 5 nm). AgNPs, silver nanoparticles; Au, gold; TEM, transmission electron microscopy; *A. squamosa*, *Annona squamosa*.

Statistical analysis. Statistical analyses were performed using GraphPad Prism version 10 (Dotmatics). Data are presented as the mean ± standard deviation (SD) from three independent experiments (n=3), unless otherwise stated. Prior to hypothesis testing, data normality was assessed using the Shapiro-Wilk test. For cell viability assays, DNA content analysis, nuclear morphometric measurements and relative gene expression analyses, statistical differences among groups were determined using one-way ANOVA, followed by Dunnett's multiple-comparisons test. Apoptosis levels between the untreated control and AgNP-treated groups were compared using an unpaired two-tailed Student's t-test. Gene expression data associated with apoptosis-related genes were analyzed using two-way ANOVA followed by Tukey's multiple-comparisons test. Differences were considered statistically significant at $P<0.05$.

Results

Synthesis and characterization of AgNPs and AuNPs. In the present study, a noticeable color transition from light brown to dark brown was observed (Fig. 1A), and a prominent plasmon resonance peak in the 410-420 nm range was detected, confirming the formation of AgNPs (the *A. squamosa* seeds extract itself did not exhibit any peaks in the 300-600 nm range) (Fig. 1B). This indicates that *A. squamosa* seeds extract is a highly effective reducing agent for converting silver ions to silver. For AuNPs, the successful synthesis was visually confirmed by a distinct purple color observed after *A. squamosa* seeds extract solution was mixed with $HAuCl_4$ solution (Fig. 1D). The plant extract efficiently reduced Au3+ ions to Au0. The UV-Vis spectroscopy analysis of the resulting colloidal solutions (Fig. 1E) revealed absorption peaks in the 520-540 nm range, consistent with the surface plasmon resonance of AuNPs, typically around 520 nm. This resonance is influenced by the size of the NPs, affirming the successful synthesis of AuNPs (30).

To further investigate the size, shape and crystal structure of the NPs, TEM and PSA analyses were employed. TEM images revealed distinct morphological characteristics of the AgNPs and AuNPs. The AgNPs (Fig. 1C) exhibited predominantly spherical morphology with moderate polydispersity and occasional particle aggregation. High-resolution (HR)TEM imaging showed well-defined lattice fringes, confirming the crystalline nature of the NPs. By contrast, the AuNPs (Fig. 1F) appeared more uniform in shape and size, displaying predominantly spherical to quasi-spherical morphologies. The HRTEM image of AuNPs revealed pronounced lattice fringes with a characteristic radial pattern, indicating high crystallinity and ordered atomic arrangements. According to the PSA analysis, the average diameter of AgNPs was 14.05 nm, with sizes ranging from 6 to 25 nm, while AuNPs had an average size of 14.92 nm, ranging from 3.67 to 44.89 nm (Fig. 2A and D). Meanwhile, measurements performed using a ViewSizer 3000 NP Size Analyzer; the mean hydrodynamic diameters of the AgNPs and AuNPs were 40.60±34 and 72.65±46 nm, respectively. For AgNPs, the D10, D50 and D90 values were 22.0, 29.5 and 70.76 nm, respectively, indicating that 10, 50 and 90% of the particles had diameters below these values. However, the D10, D50 and D90 values of AuNPs were 26.7, 61.2 and 132.6 nm, respectively (Fig. 2B and E). X-ray diffraction analysis of

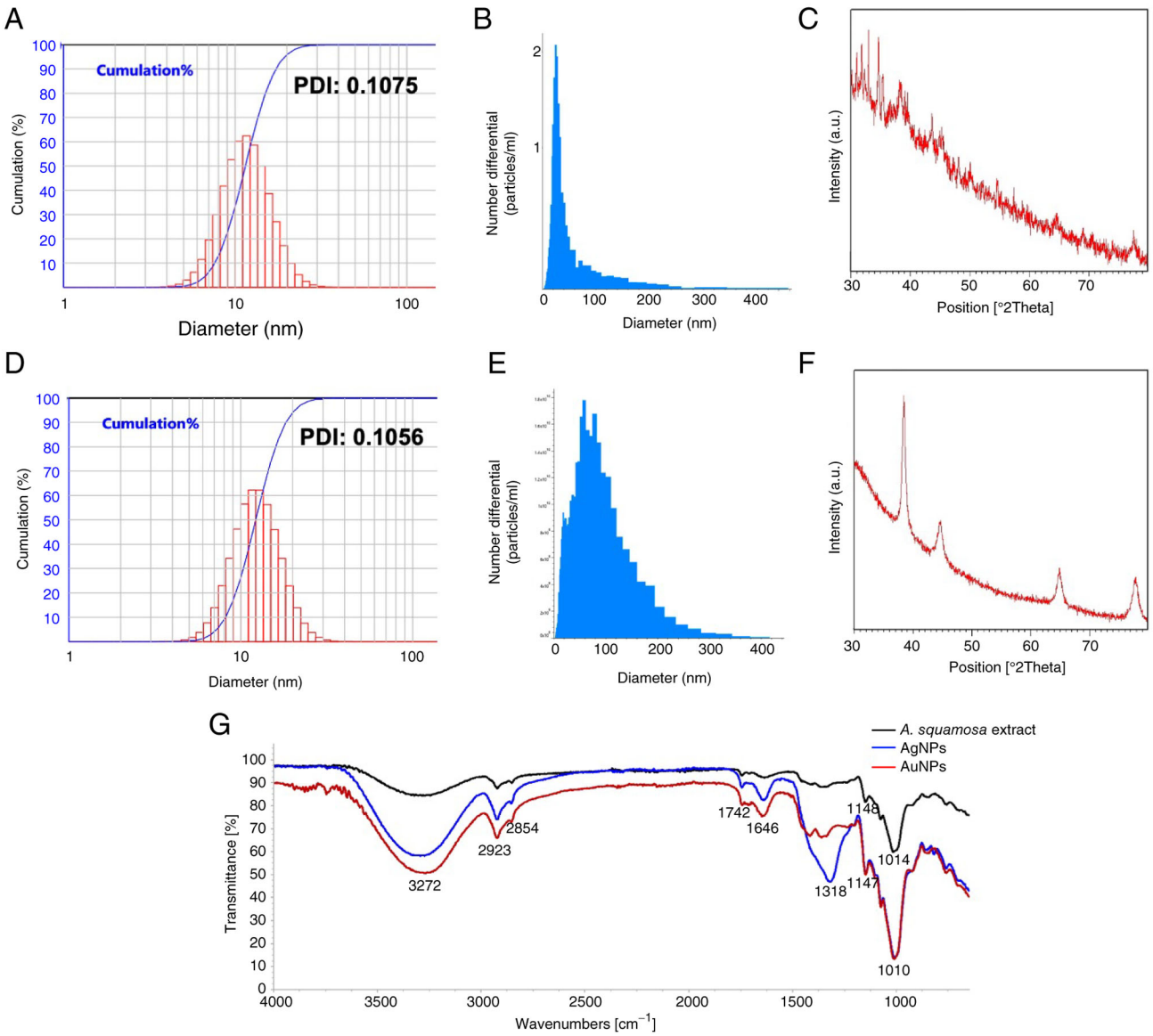

Figure 2. Size distribution XRD patterns confirm the crystalline structures of the NPs. (A) PSA result of AgNPs. (B) NP size analysis of AgNPs using ViewSizer 3000. (C) XRD patterns of AgNPs. (D) PSA result analysis of AuNPs (E). NP size analysis of AuNPs using ViewSizer 3000. (F) XRD patterns of AuNPs. (G) The fourier transform infrared (FT-IR) spectra of *A. squamosa* seed extract, AgNPs and AuNPs. AgNPs, silver nanoparticles; AuNPs, gold nanoparticles; a.u., absorption units; XRD, X-ray diffraction; PSA, particle size analyzer; PDI, polydispersity index.

the synthesized AgNPs showed broad peaks at 38.29, 45.41, 64.40 and 77.54˚, corresponding to the 111, 200, 220 and 311 planes, indicating a face-centered cubic structure. Similarly, the XRD patterns of the biologically synthesized AuNPs revealed sharp peaks at 38.20, 43.73, 64.77 and 77.72˚, which align with the 111, 200, 220 and 311 planes, confirming their face-centered cubic crystalline structure (Fig. 2C and F).

As shown in Fig. 2G, the synthesized AgNPs and AuNPs had similar peaks to *A. squamosa* seed extract, indicating that *A. squamosa* seed extract contributed to the reduction of Ag and Au ions. A broad peak was present at ~3,272/cm that comes from OH stretching, and a smaller peak at 2,923/cm from aliphatic CH. The peaks at 1,010/cm and 1,147/cm confirm the presence of secondary OH groups. These functional groups interact with the silver and gold to form a protective layer around the NPs, which keeps them from clumping together. Previous studies have shown that hydroxyl and phenolic groups tend to bind strongly to noble metals through polar and coordinating interactions (40). The increase in peak intensity and slight shifts in wavelength observed in the NPs spectrum, for example at 3,272, 1,147 and 1,010/cm, probably occur because the seed extract is coordinating with the metals (41). Of note, the AgNPs show a unique strong peak at 1,318/cm that comes from C-O aromatic ester stretching and OH bending, which was not present in *A. squamosa* seeds extract or AuNPs.

Metal content of AgNPs. ICP-OES analysis revealed that the synthesized AgNPs contained 6.60 μg/g Ag, confirming the presence of Ag in the NP preparation.

Sterility evaluation of NPs. The sterility evaluation of AgNPs demonstrated that AgNPs were sterile, as evidenced by the absence of bacterial growth following inoculation onto MHA medium (Fig. 3A; Table II).

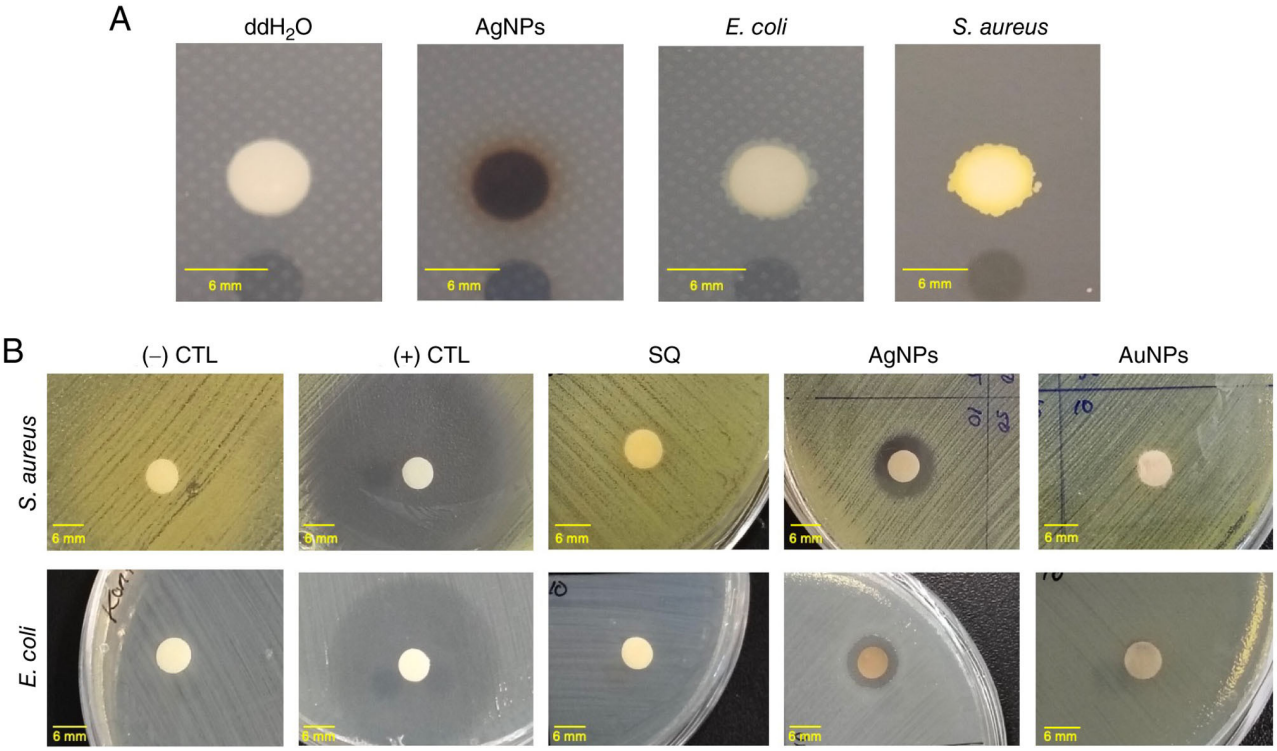

Figure 3. Sterility and antibacterial activity of the NPs. (A) Sterility test of AgNPs. (B) The antibacterial activity of AgNPs and AuNPs against *S. aureus* and *E. coli* at concentrations of 10, 25, 50 and 100 mg/ml, with a 24-h incubation period (scale bars, 6 mm). CTL, control; SQ, *A. squamosa* seed extract; AgNPs, silver nanoparticles; AuNPs, gold nanoparticles.

Table II. Sterility test of AgNPs.

Sample	Bacterial growth
AgNPs	-
S. aureus culture	+
E. coli culture	+
Sterile nuclease free water	+

AgNPs, silver nanoparticles; +, bacterial growth observed; -, bacterial growth not observed.

Antibacterial potency of AgNPs and AuNPs. To investigate the antibacterial activity of AgNPs and AuNPs, disk diffusion assays were performed against *E. coli* and *S. aureus*. Growth inhibition was observed on plates with 100, 50, 25 and 10% concentrations of 100 mg/ml AgNPs, but not with AuNPs or *A. squamosa* seeds extract (control) after 24 h of incubation. Table III and Fig. 3B reveal that *E. coli* had a smaller zone of inhibition compared to *S. aureus*. The bacterial growth inhibition around the wells was attributed to the diffusion of AgNPs to the MHA plates.

Furthermore, the MIC and MBC values of AgNPs were determined (Table IV). The MIC and MBC are important metrics in antimicrobial evaluation, indicating an agent's capacity to inhibit microbial proliferation and eradicate pathogens, respectively. By definition, the MIC represents the lowest concentration of an antimicrobial agent that prevents visible microbial growth, whereas the MBC is the lowest concentration required to kill 99.9% of the microbial population (42). The correlation between these values reveals the agent's mode of action: An MBC value close to the MIC suggests bactericidal activity, whereas a substantially higher MBC denotes a bacteriostatic effect (43). As presented in Table IV, the AgNPs exhibited antibacterial activity against both tested microorganisms. The MIC values were 0.781 mg/ml for *Staphylococcus aureus* and 3.125 mg/ml for *Escherichia coli*. The MBC values for both bacteria were 3.125 mg/ml. The lower MIC value observed for *S. aureus* indicates that AgNP was more effective against this Gram-positive bacterium than against *E. coli*, as a lower concentration was required to inhibit bacterial growth. Furthermore, the identical MBC values suggest that a concentration of 3.125 mg/ml was required to achieve bactericidal activity against both bacterial species. The AgNPs exhibited bacteriostatic activity against *S. aureus* and bactericidal activity against *E. coli*, as evidenced by the relationship between their MIC and MBC values. In *S. aureus*, the MBC was 4x higher than the MIC, whereas in *E. coli*, the MIC and MBC were identical, indicating that the inhibitory concentration was also sufficient to exert a bactericidal effect.

Effect of AgNPs, AuNPs and $AgNO_3$ on the viability of MCF-7 and 293 cells. To evaluate the anticancer activity and selective cytotoxicity of the biosynthesized NPs, an MTT assay was performed on the breast cancer cell line MCF-7 and the non-carcinogenic 293 cells. Treatment with *A. squamosa* extract alone (100 μg/ml) showed limited cytotoxic activity against MCF-7 cells at 24 h, with the cell viability remaining comparable to the control group (>90%). However, prolonged exposure significantly reduced the cell viability to ~55% at

Table III. Results of disc diffusion test of AgNPs and AuNPs.

Organism	Concentration (mg/ml)	Inhibition zone diameter, mm	
		AgNP	AuNP
Staphylococcus aureus	10	9.91±0.29	0.0
	25	11.57±0.68	0.0
	50	11.89±0.37	0.0
	100	13.63±2.86	0.0
	+ (Gentamycin)	34.43±3.40	36.45±0.42
	- (sterile ddH_2O)	0.0	0.0
	A. squamosa seeds extract all concentrations	0.0	0.0
Escherichia coli	10	8.41±0.91	0.0
	25	7.89±0.37	0.0
	50	8.28±1.10	0.0
	100	8.53±1.03	0.0
	+ (Gentamycin)	18.09±0.43	19.67±0.60
	- (sterile ddH_2O)	0.0	0.0
	A. squamosa seeds extract all concentrations	0.0	0.0

AgNPs, silver nanoparticles; Au, gold.

Table IV. MIC and the MBC values of AgNPs.

Tested bacteria	MIC value (mg/ml)	MBC value (mg/ml)
Staphylococcus aureus	0.781	3.125
Escherichia coli	3.125	3.125

MIC, minimum inhibitory concentration; MBC, minimum bactericidal concentration; AgNPs, silver nanoparticles.

both 48 and 72 h (P<0.0001), indicating a time-dependent antiproliferative effect (Fig. 4A). By contrast, AuNPs only reduced the cell viability after 24 h at 100 and 200 μg/ml. By 48 and 72 h, there was no significant difference in cell viability between the AuNP-treated cells and the control (Fig. 4B).

Treatment with $AgNO_3$ produced strong cytotoxic effects on MCF-7 cells, reducing cell viability to ~40-45% across all tested concentrations after 24 h of treatment (P<0.0001) (Fig. 4C). Among all tested treatments, AgNPs demonstrated the greatest anticancer activity against MCF-7 cells. At 24 h, AgNPs reduced cell viability in a concentration-dependent manner, with higher concentrations decreasing viability to ~55-60% (P<0.0001). The cytotoxic effect became more pronounced after 48 h, where the highest concentration reduced viability to ~25-30% (P<0.0001). Similar effects were maintained at 72 h, indicating sustained growth inhibition and enhanced anticancer activity compared with SQ and AuNPs alone (Fig. 4D).

To assess selectivity, the effects of $AgNO_3$ and AgNPs were also evaluated in 293 cells. $AgNO_3$ markedly reduced 293 cell viability, decreasing the proportion of viable cells to ~30-40% at all tested concentrations (Fig. 4E), suggesting considerable toxicity toward normal cells. By contrast, AgNPs displayed substantially lower toxicity toward 293 cells, maintaining cell viability above 70-98% across most concentrations and time-points (Fig. 4F). Although a slight decline in viability was observed at higher concentrations, the reduction was significantly less severe than that observed in MCF-7 cells.

The MTT assay results showed that while the AuNPs weren't toxic to the cells, the AgNPs had a clear effect, and accordingly, the study further focused on measuring their IC_{50} value. The IC_{50}s of the AgNPs were assessed through a detailed analysis involving five doses and three incubation periods. As shown in Fig. 5, it was found that even high doses of AgNPs did not kill enough cells to determine the IC_{50} after 24 h-it was >200 μg/ml. However, at 48 and 72 h, the AgNPs were much more effective, as evidenced by the significant reduction of cell viability. The IC_{50} values were determined to be 106.7 μg/ml at 48 h and 79.5 μg/ml at 72 h. These results show that the AgNPs have the potential to stop cancer cells from growing, suggesting they could be useful in cancer treatments.

Effect of AgNPs on the cell cycle phase and expression of several oncogenes. To investigate the possible molecular targets of AgNPs in the MCF-7 cell line, cell cycle and RT-qPCR analysis of several identified oncogenes in breast cancer (44-46) was performed, including MYC, HER2, CCND1 and COX-2. The DNA content analysis revealed that AgNPs treatment significantly reduced the percentage of cells below 2N and increased the number of cells with 4N DNA. The RT-qPCR analysis results indicated that AgNPs derived from *A. squamosa* seed extract effectively reduced the mRNA levels of MYC, CCND1, HER2, COX-2 and CTNND1 (Fig. 6). The Cq values are presented in Table SI. These findings

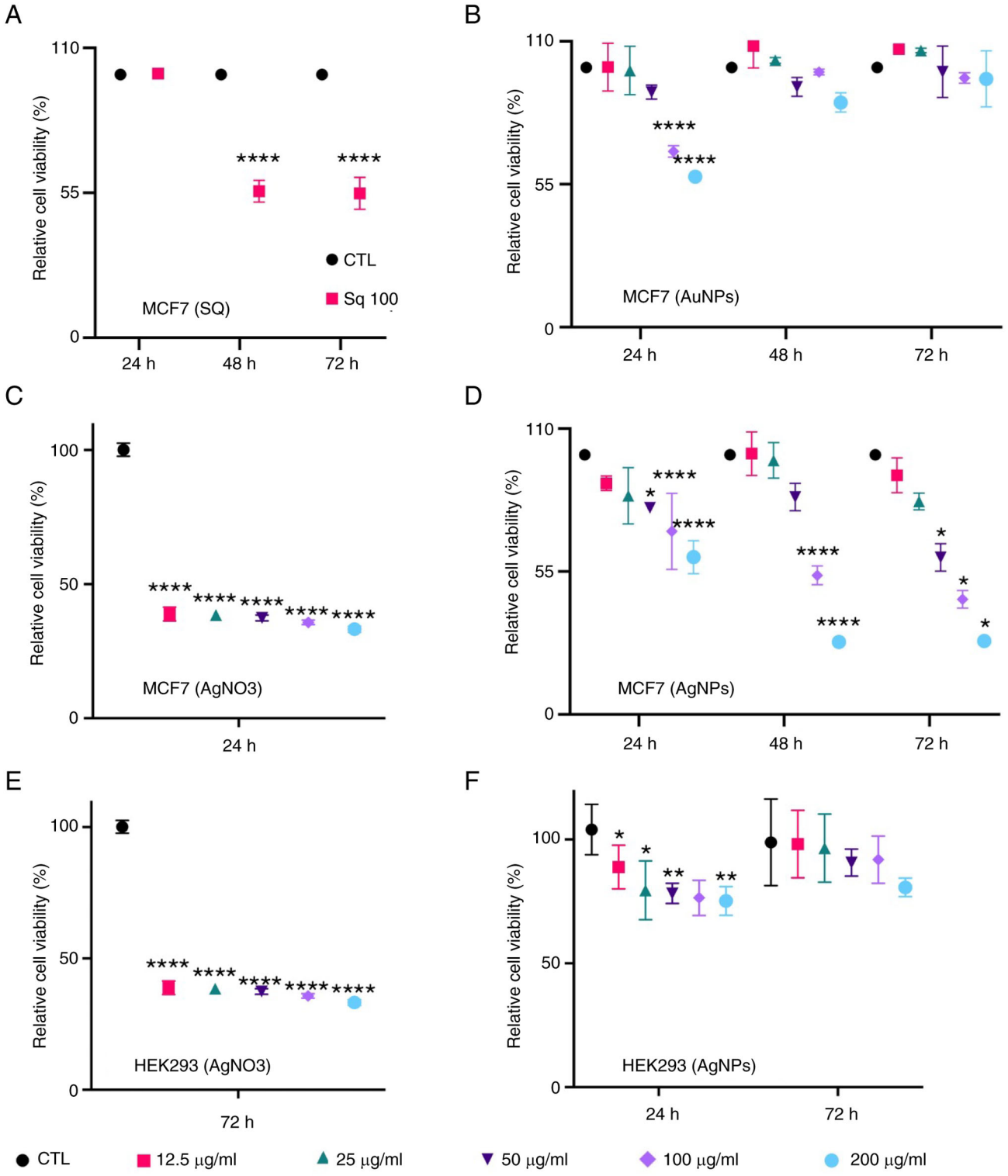

Figure 4. Effects of *Annona squamosa* seed extract and silver- or gold-based formulations on the viability of MCF-7 and 293 cells. (A) Viability of MCF-7 cells following treatment with SQ for 24, 48 and 72 h. (B) Viability of MCF-7 cells following treatment with AuNPs synthesized using *A. squamosa* seed extract at various concentrations for 24, 48 and 72 h. (C) Viability of MCF-7 cells following treatment with $AgNO_3$ at various concentrations for 24 h. (D) Viability of MCF-7 cells following treatment with AgNPs synthesized using *A. squamosa* seed extract at various concentrations for 24, 48 and 72 h. (E) Viability of 293 cells following treatment with $AgNO_3$ at various concentrations for 72 h. (F) Viability of 293 cells following treatment with AgNPs at various concentrations for 24 and 72 h. Data are presented as the mean ± standard deviation from three independent experiments (n=3). Statistical significance was determined using one-way ANOVA, with comparisons made against the untreated control group. Asterisks indicate significant differences: *P<0.05, **P<0.01 and ****P<0.0001 vs. CTL. CTL, control; SQ, *A. squamosa* seed extract; AgNPs, silver nanoparticles; AuNPs, gold nanoparticles.

underscore the potential of AgNPs to modulate the expression of critical oncogenes and offer valuable insights into their anti-proliferative mechanisms in cancer cells.

AgNPs induce apoptosis in MCF-7 cells. To investigate whether the cytotoxic effect of AgNPs was associated with apoptosis, MCF-7 cells were treated with AgNPs (100 µg/ml)

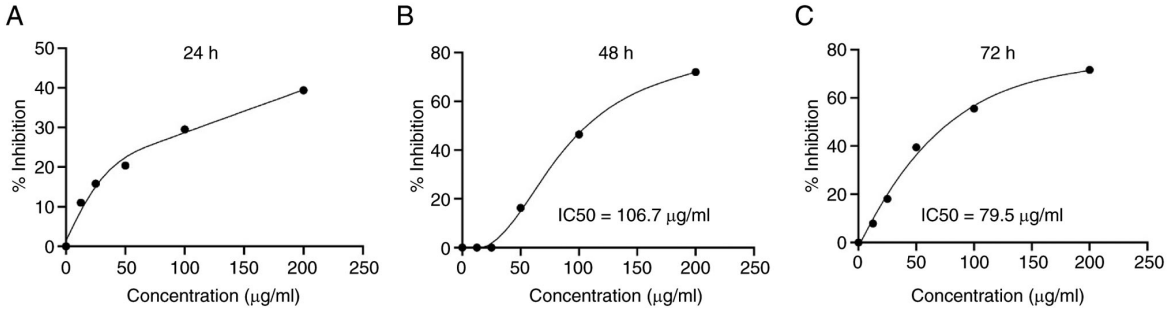

Figure 5. IC_{50} of silver nanoparticles prepared with *A. squamosa* seeds extract against the MCF7 cell line after (A) 24, (B) 48 and (C) 72 h of treatment.

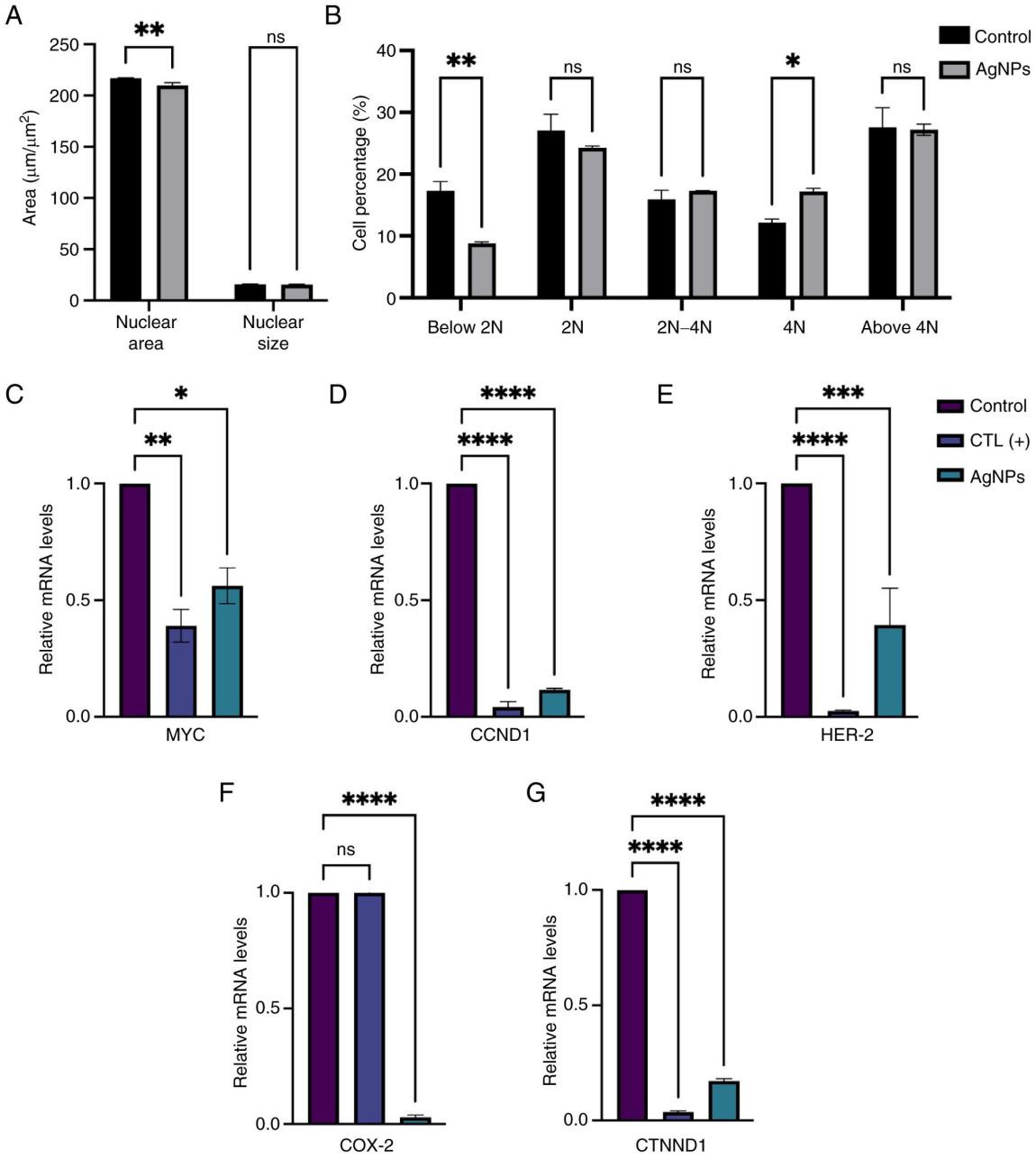

Figure 6. AgNPs treatment alters cell cycle phase and several oncogene expressions in MCF-7 cells. (A) The nuclear size and nuclear area of the MCF-7 cells following treatment with 100 μg/ml of AgNPs for 24 h. (B) The DNA content represents cell cycle phase of MCF-7 cells following treatment with 100 μg/ml of AgNPs for 24 h. (C) Relative mRNA levels of MYC, (D) CCND1, (E) HER-2, (F) COX-2 and (G) CTNND1 in MCF-7 cells following treatment with AgNPs (100 μg/ml) for 48 h. Data are presented as mean ± standard deviation of three independent replicates (n=3). Statistical analysis was performed using one-way ANOVA. Asterisks indicate statistically significant differences compared with the control group: *P<0.05, **P<0.01, ***P<0.001 and ****P<0.0001 vs. CTL. ns, no significance; CTL, control; MYC, c-Myc; CCND1, cyclin D1; HER2, human epidermal growth factor receptor-2; COX-2, cyclooxygenase-2, CTNND1, catenin delta-1; AgNPs, silver nanoparticles.

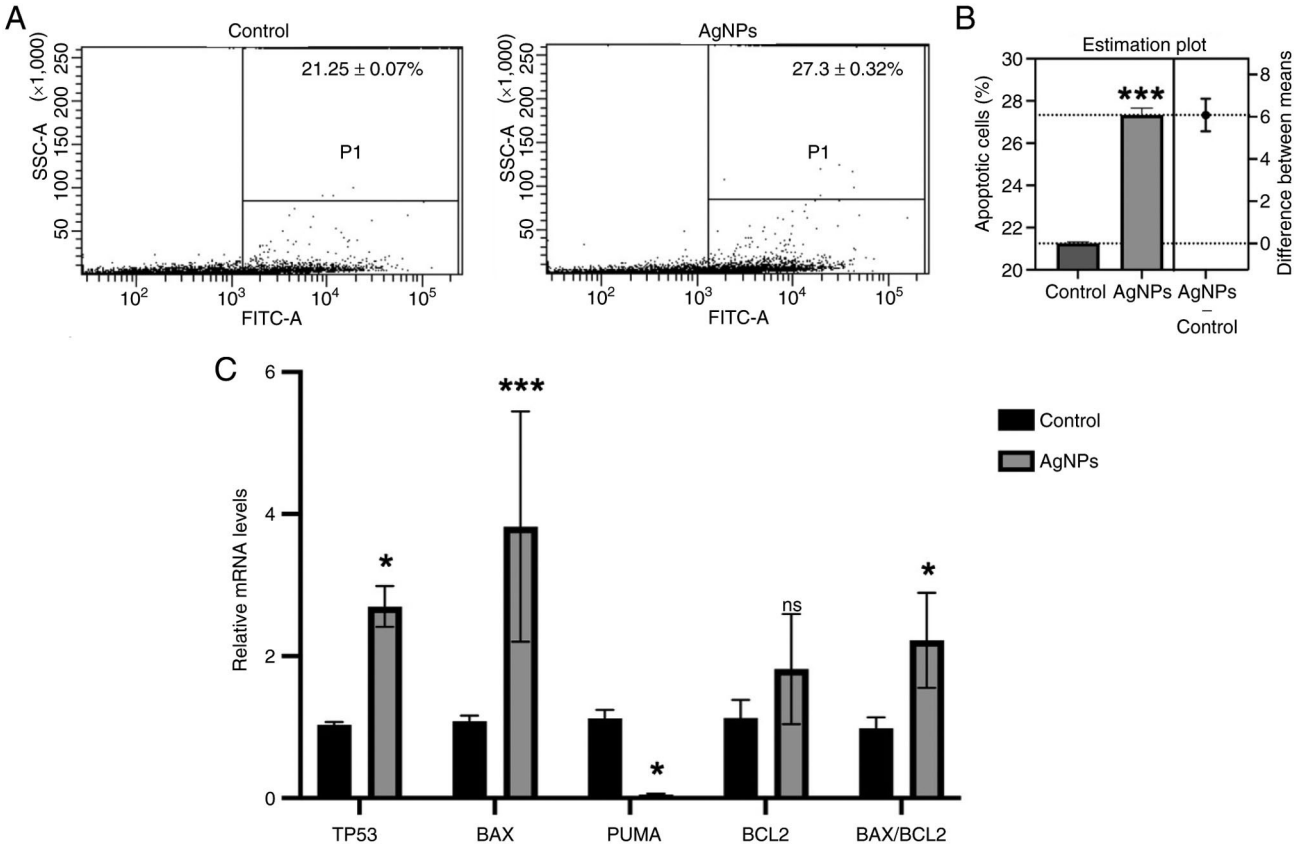

Figure 7. AgNP treatment induces apoptosis and modulates the expression of apoptosis-related genes in MCF-7 cells. (A) Representative flow cytometry dot plots of Annexin V-FITC-stained MCF-7 cells showing apoptotic populations in the untreated control and AgNP-treated (100 μg/ml, 48 h) groups. (B) Quantification of apoptotic cells demonstrating a significant increase in apoptosis following AgNP treatment compared with the control group, as determined by Student's t-test. (C) Relative expression levels of apoptosis-related genes following AgNP exposure. AgNP treatment significantly upregulated p53, BAX and BAX/BCL2 ratio, while significantly downregulating PUMA expression compared with the control. Gene expression data were analyzed using two-way ANOVA and are presented as the mean ± standard deviation from three independent experiments (n=3). Statistical significance is indicated as *P<0.05 and ***P<0.001 vs. control. ns, not significant; AgNPs, silver nanoparticles; TP53, tumor protein P53; BAX, BCL2 associated X; BBC3/PUMA, BCL2 binding component 3; BCL2, BCL2 apoptosis regulator.

for 48 h and analyzed using Annexin V-FITC flow cytometry. As shown in Fig. 7A and B, AgNP treatment markedly increased the population of Annexin V-positive cells compared with the untreated control. Quantitative analysis revealed that the percentage of apoptotic cells increased significantly from 21.25±0.07% in the control group to 27.3±0.32% following AgNP treatment (P<0.001; Fig. 7B), indicating that AgNPs effectively induced apoptosis in MCF-7 cells.

To further elucidate the molecular mechanisms underlying AgNP-induced apoptosis, the expression of several apoptosis-related genes was evaluated by RT-qPCR (Fig. 7C), and the ΔΔCt values are presented in Table SII. AgNP treatment significantly upregulated the expression of p53 (2.7-fold), BAX (3.8-fold), and the BAX/BCL2 ratio (2.2-fold) relative to the control group (P<0.05-0.001). By contrast, the expression of PUMA was markedly reduced to ~0.05-fold of the control level (P<0.05). These findings suggest that AgNPs induce apoptosis in MCF-7 cells through activation of the p53-mediated apoptotic pathway.

Discussion

AgNPs are increasingly valued for their antimicrobial properties in medical applications. Although the precise mechanism behind the antibacterial activity of AgNPs is still being studied, it is thought that both the size of the NPs and the presence of phytochemical components contribute synergistically to their effectiveness. The extensive surface area and diverse phytochemical constituents of the seed extract facilitate the reduction and stabilization of AgNPs, which are typically <100 nm in size (47). AgNPs can disrupt bacterial cells through various mechanisms, including electrostatic interactions with the negatively charged bacterial membranes, which leads to cell death (48). This interaction induces oxidative stress through reactive oxygen species within the cell membrane (49,50). The AgNPs don't stop there-they actually break through the bacterial membrane, disrupt respiratory chains and enter organelles where Ag^{+} ions interact with DNA, ribosomes and enzymes. Of note, AgNPs prefer to attach to nucleosides rather than phosphate groups, which leads to DNA damage and ultimately cell death. AgNPs also accumulate in the membranes of *E. coli* and *S. aureus*, increasing membrane permeability and causing cell death.

Research utilizing *Tectona grandis* seed extract for AgNP synthesis has revealed that NPs ranging from 10 to 30 nm in size can substantially inhibit *S. aureus* and *E. coli* (51). In another study, AgNPs produced using *Trigonella foenum-graecum* seed extract demonstrated MIC values of 62.5 μg/ml for

S. aureus and 125 μg/ml for *E. coli* (52). While earlier studies have generally reported larger inhibition zones for *E. coli* compared to *S. aureus* (52), the present findings indicate that AgNPs exhibit greater effectiveness against *S. aureus*. Meanwhile, a previous study on AgNPs synthesized using an aqueous extract of *Hypericum perforatum* L. reported bactericidal activity against *S. aureus* based on MIC and MBC evaluations (53), which contrasts the present findings, where a bacteriostatic effect was observed. This discrepancy highlights the impact of the specific plant extract used in AgNP synthesis on their antibacterial performance.

In addition to their antibacterial activity, the present study demonstrated that AgNPs exert a selective antiproliferative effect against cancer cells while exhibiting minimal cytotoxicity toward normal 293 cells. This selective cytotoxicity is highly desirable for anticancer agents, as it minimizes damage to healthy tissues. Similar findings have been reported previously, where AgNPs synthesized using walnut green husk extract showed substantially greater cytotoxicity toward MCF-7 breast cancer cells than toward non-cancerous L-929 fibroblasts (54). The preferential toxicity of AgNPs toward cancer cells has been attributed to their enhanced cellular uptake, which is facilitated by the altered metabolism, rapid proliferation and increased endocytic activity characteristic of malignant cells. These biological features render cancer cells more susceptible to NP-induced oxidative stress and cellular damage than normal cells (55).

Of note, the present results revealed a clear difference between $AgNO_3$ and AgNPs. While $AgNO_3$ exhibited cytotoxic effects on both MCF-7 and 293 cells, AgNPs selectively inhibited the growth of cancer cells with limited toxicity toward normal cells. This selectivity may be attributed to the controlled and sustained release of Ag^+ ions from the NP matrix, in contrast to the immediate availability of free Ag^+ ions from $AgNO_3$. Furthermore, the acidic tumor microenvironment likely contributes to the enhanced anticancer activity of AgNPs (56). Cancer cells generally maintain a lower extracellular pH than normal cells, which promotes increased dissolution of AgNPs and consequently a higher release of Ag^+ ions within tumor tissues. As a result, cancer cells are exposed to greater intracellular silver ion concentrations, leading to elevated oxidative stress, mitochondrial dysfunction and apoptosis, while normal cells experience comparatively lower toxicity (57). These mechanisms collectively support the selective anticancer potential of AgNPs observed in this study.

The anticancer activity of AgNPs may also be associated with their ability to modulate the expression of genes involved in cell proliferation and survival. In the present study, dose-dependent cytotoxicity on MCF-7 cells treated with AgNPs was observed, with IC_{50} values of 106.7 μg/ml at 48 h and 79.5 μg/ml at 72 h. These IC_{50} values are higher than those found in a previous study, which reported IC_{50} values of 50 μg/ml at 24 h and 30 μg/ml at 48 h for AgNPs synthesized using *A. squamosa* leaf extract against MCF-7 cells (24). The differences might be attributed to the use of *A. squamosa* seed extract.

Another mechanism underlying the anticancer activity of AgNPs is their ability to induce apoptosis in cancer cells. In the present study, AgNP treatment significantly increased the proportion of apoptotic MCF-7 cells compared with the control group, indicating that apoptosis contributes to the observed cytotoxic effect. This response is likely mediated through activation of p53, a key regulator of programmed cell death. Similar findings have been reported for green-synthesized AgNPs from *Allium ampeloprasum*, which increased p53 and BAX expression while decreasing BCL2 expression (58). Although BCL2 expression was also elevated in the present study, the increase in BAX expression was substantially greater, resulting in a higher BAX/BCL2 ratio. This ratio is widely recognized as a key indicator of apoptosis, reflecting the balance between pro-apoptotic and anti-apoptotic signaling. Therefore, the elevated BAX/BCL2 ratio observed in AgNP-treated cells supports the conclusion that AgNPs induce apoptosis through activation of the intrinsic mitochondrial apoptotic pathway (59).

When MCF-7 cells were exposed to AgNPs, significant changes in several cancer-related genes were observed in the present study. The treatment notably decreased the expression of *MYC*, *CCND1*, *COX-2*, *HER2* and *CTNND1*. This is particularly interesting because c-Myc plays a crucial role in driving breast cancer growth-it helps cancer cells divide rapidly, and when it's overactive, patients tend to have worse outcomes (60). c-Myc promotes cell cycle progression by activating CCND1, which is frequently overexpressed and amplified in breast cancer. CCND1 functions in the nucleus to regulate the transition from G1 to S phase by interacting with CDK4 and CDK6 (61). Meanwhile, COX-2 is often overexpressed in breast cancer and its overexpression contributes to tumor growth, invasion and metastasis (62). AgNPs effectively decreased *HER*2 levels. HER2's role in breast cancer is particularly concerning since it acts together with other EGFR family proteins to trigger pathways that drive tumor growth and spread (63). A previous study reported lower CTNND1 expression in breast cancer tissues from patients with breast cancer compared to mammary gland cells from non-tumor patients (64). This study is the first to demonstrate that AgNPs synthesized with *A. squamosa* seed extract can modulate several breast cancer-related genes. Although AgNPs have good anticancer activity against MCF-7 cells, it is still necessary to conduct further analyses to see the effectiveness of AgNPs in animal models (*in vivo* studies).

Despite the strong anticancer and antibacterial effects of AgNPs, AuNPs synthesized using *A. squamosa* seed extract did not exhibit comparable bioactivities. The differences in the physicochemical properties of these nanomaterials may have influenced their biological performance. Similar observations have been reported in previous studies, where AuNPs showed minimal or no cytotoxic effects in HeLa cells (65), A549 and Vero cells (66) and Caco-2 cells (67). The low cytotoxicity observed in the present study suggests that *A. squamosa*-generated AuNPs may have potential for biomedical applications where biocompatibility is desirable. However, further studies are required to evaluate their loading capacity, stability, targeting ability and delivery efficiency before their suitability as drug-delivery vehicles can be established. In general, AuNPs have attracted considerable interest in drug-delivery research because of their tunable size and shape, ease of surface functionalization and ability to interact with a wide range of biomolecules.

Previous studies have explored the use of AuNPs for the delivery of drugs, genes, proteins and vaccines (68-73). Therapeutic agents, including antibiotics, can be associated with AuNPs through ionic interactions, covalent conjugation or physical adsorption.

Future studies should evaluate the anticancer efficacy of the synthesized silver and gold NPs in additional breast cancer subtypes, particularly triple-negative breast cancer (MDA-MB-231), to determine whether their therapeutic effects extend beyond hormone receptor-positive breast cancer. Preclinical *in vivo* studies using appropriate animal models should then assess antitumor efficacy, biodistribution, pharmacokinetics and long-term safety, including the absorption, distribution, metabolism and excretion profiles of the NPs. These studies will be essential for establishing optimal dosing regimens, evaluating systemic toxicity associated with prolonged exposure and supporting the clinical translation of NP-based therapies. In addition, addressing public perception and ethical considerations, together with collaboration among researchers, clinicians and regulatory agencies, will facilitate the safe and effective development of silver- and gold-based nanomedicines.

In conclusion, *A. squamosa* seed extract successfully mediated the green synthesis of AgNPs and AuNPs with nanoscale size, spherical morphology and crystalline structures. Among the synthesized NPs, the AgNPs exhibited bacteriostatic activity against *S. aureus* and bactericidal activity against *E. coli*, whereas the AuNPs showed no detectable antibacterial effect. The AgNPs also demonstrated selective anticancer activity by inhibiting the proliferation of MCF-7 breast cancer cells while exerting minimal toxicity toward normal 293 cells. The cytotoxic effect was dose- and time-dependent, with IC_{50} values of 106.704 and 79.519 μg/ml after 48 and 72 h of treatment, respectively. Mechanistically, AgNPs modulated the expression of cancer-related genes, suppressed the expression of several oncogenes and induced apoptosis through the activation of p53-associated pathways, as evidenced by increased apoptotic cell populations and an elevated BAX/BCL2 ratio. While these findings underscore the therapeutic potential of *A. squamosa* seed extract-biosynthesized NPs, further *in vivo* studies are required to elucidate their biodistribution, pharmacokinetics, mechanisms of action and long-term safety. Multidisciplinary collaborations will be essential to advance their translation into clinical applications.

Acknowledgements

The authors are grateful to Mr. Bryan Khalfani, Bachelor of Science (B.Sc) and Mr. Muhammad Sanda Amanullah, B.Sc from the Biology Department, Faculty of Science and Technology, Universitas Airlangga (Surabaya, Indonesia) for their technical assistance with measuring inhibition zone diameters during antibacterial analysis.

Funding

This research was supported by the International Research Consortium (IRCON) 2024, Universitas Airlangga, Indonesia (grant no. 178/UN3.LPPM/PT.01.03/2024) and Universiti Malaya research grant (grant no. IF033-2024).

Availability of data and materials

The data generated in the present study are included in the figures and/or tables of this article.

Authors' contributions

FRPD contributed to the conception of the study, acquisition of data, analysis and interpretation of data, confirmation of the authenticity of the raw data, manuscript preparation and funding acquisition. AUR and AR contributed to performing the experiments, and the acquisition and analysis of data. AG confirmed the authenticity of the raw data and data analysis. AKMJ contributed to funding acquisition, data acquisition and manuscript preparation. TD contributed to the data analysis and manuscript preparation. VRH and ACE contributed to performing the experiments, data acquisition and analysis. All authors read and approved the manuscript and agree to be accountable for all aspects of the research, ensuring that any issues related to the accuracy or integrity of any part of the work were appropriately investigated and resolved.

Ethics approval and consent to participate

Not applicable.

Patient consent for publication

Not applicable.

Competing interests

The authors declare that they have no competing interests.

Use of artificial intelligence tools

During the preparation of this work, AI tools (ChatGPT-5.5; https://chatgpt.com) were used to improve the readability and language of the manuscript, and subsequently, the authors revised and edited the content produced by the AI tools as necessary, taking full responsibility for the ultimate content of the present manuscript.

References

1. Antunes Filho S, Dos Santos MS, Dos Santos OAL, Backx BP, Soran ML, Opriş O, Lung I, Stegarescu A and Bououdina M: Biosynthesis of nanoparticles using plant extracts and essential oils. Molecules 28: 3060, 2023.
2. Dewi FRP, Lim V, Rosyidah AL, Fatimah F, Wahyuningsih SPA and Zubaidah U: Characterization of silver nanoparticles (AgNPs) synthesized from Piper ornatum leaf extract and its activity against food borne pathogen *Staphylococcus aureus*. Biodivers J Biol Divers 24: 1742-1748, 2023.
3. Rashmi V and Sanjay KR: Green synthesis, characterisation and bioactivity of plant-mediated silver nanoparticles using Decalepis hamiltonii root extract. IET Nanobiotechnol 11: 247-254, 2017.
4. Al-Radadi NS, Al-Bishri WM, Salem NA and ElShebiney SA: Plant-mediated green synthesis of gold nanoparticles using an aqueous extract of Passiflora ligularis, optimization, characterizations, and their neuroprotective effect on propionic acid-induced autism in Wistar rats. Saudi Pharm J 32: 101921, 2024.

5. Beeram SR, Rodriguez E, Doddavenkatanna S, Li Z, Pekarek A, Peev D, Goerl K, Trovato G, Hofmann T and Hage DS: Nanomaterials as stationary phases and supports in liquid chromatography. Electrophoresis 38: 2498-2512, 2017.
6. Stark WJ, Stoessel PR, Wohlleben W and Hafner A: Industrial applications of nanoparticles. Chem Soc Rev 44: 5793-5805, 2015.
7. Subbiah R, Veerapandian M and Yun KS: Nanoparticles: Functionalization and multifunctional applications in biomedical sciences. Curr Med Chem 17: 4559-4577, 2010.
8. Frey NA, Peng S, Cheng K and Sun S: Magnetic nanoparticles: synthesis, functionalization, and applications in bioimaging and magnetic energy storage. Chem Soc Rev 38: 2532-2542, 2009.
9. Bloise N, Strada S, Dacarro G and Visai L: Gold nanoparticles contact with cancer cell: A brief update. Int J Mol Sci 23: 7683, 2022.
10. Bishoyi AK, Nouri S, Hussen A, Bayani A, Khaksari MN and Soleimani Samarkhazan H: Nanotechnology in leukemia therapy: Revolutionizing targeted drug delivery and immune modulation. Clin Exp Med 25: 166, 2025.
11. Arockiya Aarthi Rajathi F, Arumugam R, Saravanan S and Anantharaman P: Phytofabrication of gold nanoparticles assisted by leaves of *Suaeda monoica* and its free radical scavenging property. J Photochem Photobiol B 135: 75-80, 2014.
12. Tahir K, Nazir S, Li B, Khan AU, Khan ZUH, Gong PY, Khan SU and Ahmad A: *Nerium oleander* leaves extract mediated synthesis of gold nanoparticles and its antioxidant activity. Mat Lett 156: 198-201, 2015.
13. Jadoun S, Arif R, Jangid NK and Meena RK: Green synthesis of nanoparticles using plant extracts: A review. Environ Chem Lett 19: 355-374, 2020.
14. Gahlawat G and Choudhury AR: A review on the biosynthesis of metal and metal salt nanoparticles by microbes. RSC Adv 9: 12944-12967, 2019.
15. Velusamy P, Kumar GV, Jeyanthi V, Das J and Pachaiappan R: Bio-inspired green nanoparticles: Synthesis, mechanism, and antibacterial application. Toxicol Res 32: 95-102, 2016.
16. Nath D and Banerjee P: Green nanotechnology-a new hope for medical biology. Environ Toxicol Pharmacol 36: 997-1014, 2013.
17. Mohandoss S, Velu KS, Manoharadas S, Ahmad N, Palanisamy S, You S, Akhtar MS and Lee YR: Synthesis, characterization, and evaluation of silver nanoparticle-loaded carboxymethyl chitosan with sulfobetaine methacrylate hydrogel nanocomposites for biomedical applications. Polymers (Basel) 16: 1513, 2024.
18. Thakur N, Manna P and Das J: Synthesis and biomedical applications of nanoceria, a redox active nanoparticle. J Nanobiotechnology 17: 84, 2019.
19. Wahab MA, Luming L, Matin MA, Karim MR, Aijaz MO, Alharbi HF, Abdala A and Haque R: Silver micro-nanoparticle-based nanoarchitectures: Synthesis routes, biomedical applications, and mechanisms of action. Polymers (Basel) 13: 2870, 2021.
20. Khan SA, Shahid S and Lee CS: Green synthesis of gold and silver nanoparticles using leaf extract of clerodendrum inerme; characterization, antimicrobial, and antioxidant activities. Biomolecules 10: 835, 2020.
21. Bharadwaj KK, Rabha B, Pati S, Sarkar T, Choudhury BK, Barman A, Bhattacharjya D, Srivastava A, Baishya D, Edinur HA, *et al*: Green synthesis of gold nanoparticles using plant extracts as beneficial prospect for cancer theranostics. Molecules 26: 6389, 2021.
22. Jibrin F, Fanoro OT, Maluleke R, Lebepe TC, Mgedle N, Mbaz GIM, Aladesuyi OA, Kalimuthu R, Odeku OA and Oluwafemi OS: Biosynthesis, characterization, and antibacterial activity of gold, silver, and bimetallic nanoparticles using *Annona squamosa* L. leaves. Antibiotics (Basel) 13: 1199, 2024.
23. Malik M, Iqbal MA, Malik M, Raza MA, Shahid W, Choi JR and Pham PV: Biosynthesis and characterizations of silver nanoparticles from *Annona squamosa* leaf and fruit extracts for size-dependent biomedical applications. Nanomaterials (Basel) 12: 616, 2022.
24. Vivek R, Thangam R, Muthuchelian K, Gunasekaran P, Kaveri K and Kannan S: Green biosynthesis of silver nanoparticles from *Annona squamosa* leaf extract and its in vitro cytotoxic effect on MCF-7 cells. Process Biochem 47: 2405-2410, 2012.
25. VA M, Ramesh S and Muthukrishnan L: Facile fabrication of *Annona squamosa* L. seed extract mediated silver nanoparticles challenged against biofilm forming oral pathogens. Plant Nano Biol 3: 100023, 2022.
26. Jose V, Raphel L, Aiswariya KS and Mathew P: Green synthesis of silver nanoparticles using *Annona squamosa* L. seed extract: Characterization, photocatalytic and biological activity assay. Bioprocess Biosyst Eng 44: 1819-1829, 2021.
27. Miao Y, Xu X, Yuan F, Shi Y, Chen Y, Chen J and Li X: Four cytotoxic annonaceous acetogenins from the seeds of *Annona squamosa*. Nat Prod Res 30: 1273-1279, 2016.
28. Mokhtar FA, Selim NM, Elhawary SS, Abd El Hadi SR, Hetta MH, Albalawi MA, Shati AA, Alfaifi MY, Elbehairi SEI, Fahmy LI and Ibrahim RM: Green biosynthesis of silver nanoparticles using annona glabra and *Annona squamosa* extracts with antimicrobial, anticancer, apoptosis potentials, assisted by in silico modeling, and metabolic profiling. Pharmaceuticals (Basel) 15: 1354, 2022.
29. Gangapuram BR, Bandi R, Alle M, Dadigala R, Kotu GM and Guttena V: Microwave assisted rapid green synthesis of gold nanoparticles using *Annona squamosa* L peel extract for the efficient catalytic reduction of organic pollutants. J Mol Struct 1167: 305-315, 2018.
30. Huang W, Wang L, Long D and Liu X: Colorimetric determination and recycling of gold(III) ions using label-free plasmonic $H_{0.3}MoO_3$ nanoparticles. Microchimica Acta 190: 245, 2023.
31. Shahid M, Zhou Y, Cheng XW, Zar MS, Chen G and Tang RC: Ferulic acid promoted in-situ generation of AgNPs@silk as functional colorants. J Clean Prod 176: 736-744, 2018.
32. Lewis II JS: CLSI M100-Ed35 performance standards for antimicrobial susceptibility testing standards. 35th Edition. Clinical and Laboratory Standards Institute, 2025.
33. Twardowska M, Łyskowski A, Misiorek M, Szymaszek Ż, Wołowiec S, Dąbrowska M and Uram Ł: Human embryonic kidney HEK293 cells as a model to study SMVT-independent transport of biotin and biotin-furnished nanoparticles in targeted therapy. Int J Mol Sci 26: 1594, 2025.
34. Hua Z, Zhan Y, Zhang S, Dong Y, Jiang M, Tan F, Liu Z, Thiele CJ and Li Z: P53/PUMA are potential targets that mediate the protection of brain-derived neurotrophic factor (BDNF)/TrkB from etoposide-induced cell death in neuroblastoma (NB). Apoptosis 23: 408-419, 2018.
35. Cao H and Sethumadhavan K: Identification of Bcl2 as a stably expressed qPCR reference gene for human colon cancer cells treated with cottonseed-derived gossypol and bioactive extracts and bacteria-derived lipopolysaccharides. Molecules 27: 7560, 2022.
36. Zerbib J, Ippolito MR, Eliezer Y, De Feudis G, Reuveni E, Savir Kadmon A, Martin S, Viganò S, Leor G, Berstler J, *et al*: Human aneuploid cells depend on the RAF/MEK/ERK pathway for overcoming increased DNA damage. Nat Commun 15: 7772, 2024.
37. Dewi FR, Rohmatika AU, Jamil AK, Demircan T, Idris MF, Litazkiyyah L, Fahmi M, Rosyidah A, Hayati A and Sugiharto S: Plant-based synthesis of gold and silver nanoparticles using Artocarpus heterophyllus aqueous leaf extract and its anticancer activities. Narra J 5: e1770, 2025.
38. Dewi FRP, Geraldi A, Rohmatika AU, Satar M, Hajar V, You YH, Elfentiana AC and Tan SC: Phytochemical-mediated synthesis of silver and gold nanoparticles from Piper ornatum: Characterization, antibacterial efficacy, and anticancer mechanisms. J Nanotechnol 2026: 1225355, 2026.
39. Livak KJ and Schmittgen TD: Analysis of relative gene expression data using real-time quantitative PCR and the 2(-Delta Delta C(T)) method. Methods 25: 402-408, 2001.
40. Francis S, Joseph S, Koshy EP and Mathew B: Microwave assisted green synthesis of silver nanoparticles using leaf extract of elephantopus scaber and its environmental and biological applications. Artif Cells Nanomed Biotechnol 46: 795-804, 2018.
41. Baba IA, Awe OB, Mustapha S, Abubakar MA, Abdulkareem AS, Tijani JO and Obayomi KS: Influence of plant-derived extracts on the synthesis, physicochemical properties, and applications of metal and metal oxide nanoparticles. Hybrid Adv 13: 100666, 2026.
42. Geraldi A, Wardana AP, Aminah NS, Kristanti AN, Sadila AY, Wijaya NH, Wijaya MRA, Diningrum NID, Hajar VR and Manuhara YSW: Tropical medicinal plant extracts from indonesia as antifungal agents against Candida Albicans. Front Biosci (Landmark Ed) 27: 274, 2022.
43. Rodríguez-Melcón C, Alonso-Calleja C, García-Fernández C, Carballo J and Capita R: Minimum inhibitory concentration (MIC) and minimum bactericidal concentration (MBC) for twelve antimicrobials (biocides and antibiotics) in eight strains of Listeria monocytogenes. Biology (Basel) 11: 46, 2021.

44. Lin K, Baritaki S, Vivarelli S, Falzone L, Scalisi A, Libra M and Bonavida B: The breast cancer protooncogenes HER2, BRCA1 and BRCA2 and their regulation by the iNOS/NOS2 axis. Antioxidants (Basel) 11: 1195, 2022.
45. Lee EYHP and Muller WJ: Oncogenes and tumor suppressor genes. Cold Spring Harb Perspect Biol 2: a003236, 2010.
46. Majumder M, Dunn L, Liu L, Hasan A, Vincent K, Brackstone M, Hess D and Lala PK: COX-2 induces oncogenic micro RNA miR655 in human breast cancer. Sci Rep 8: 327, 2018.
47. Selvaraj V, Sagadevan S, Muthukrishnan L, Johan MR and Podder J: Eco-friendly approach in synthesis of silver nanoparticles and evaluation of optical, surface morphological and antimicrobial properties. J Nanostruct Chem 9: 153-162, 2019.
48. Dibrov P, Dzioba J, Gosink KK and Häse CC: Chemiosmotic mechanism of antimicrobial activity of Ag(+) in vibrio cholerae. Antimicrob Agents Chemother 46: 2668-2670, 2002.
49. Niño-Martínez N, Salas Orozco MF, Martínez-Castañón GA, Torres Méndez F and Ruiz F: Molecular mechanisms of bacterial resistance to metal and metal oxide nanoparticles. Int J Mol Sci 20: 2808, 2019.
50. Bhardwaj AK, Shukla A, Mishra RK, Singh SC, Mishra V, Uttam KN, Singh MP, Sharma S and Gopal R: Power and time dependent microwave assisted fabrication of silver nanoparticles decorated cotton (SNDC) fibers for bacterial decontamination. Front Microbiol 8: 330, 2017.
51. Rautela A, Rani J and Debnath M: Green synthesis of silver nanoparticles from *Tectona grandis* seeds extract: Characterization and mechanism of antimicrobial action on different microorganisms. J Anal Sci Technol 10: 5, 2019.
52. Varghese R, Almalki MA, Ilavenil S, Rebecca J and Choi KC: Silver nanopaticles synthesized using the seed extract of *Trigonella foenum-graecum* L. and their antimicrobial mechanism and anticancer properties. Saudi J Biol Sci 26: 148-154, 2019.
53. Alahmad A, Al-Zereini WA, Hijazin TJ, Al-Madanat OY, Alghoraibi I, Al-Qaralleh O, Al-Qaraleh S, Feldhoff A, Walter JG and Scheper T: Green synthesis of silver nanoparticles using *Hypericum perforatum* L. aqueous extract with the evaluation of its antibacterial activity against clinical and food pathogens. Pharmaceutics 14: 1104, 2022.
54. Khorrami S, Zarrabi A, Khaleghi M, Danaei M and Mozafari MR: Selective cytotoxicity of green synthesized silver nanoparticles against the MCF-7 tumor cell line and their enhanced antioxidant and antimicrobial properties. Int J Nanomedicine 13: 8013-8024, 2018.
55. Cairns RA, Harris IS and Mak TW: Regulation of cancer cell metabolism. Nat Rev Cancer 11: 85-95, 2011.
56. Ashby BS: pH studies in human malignant tumours. Lancet 2: 312-315, 1966.
57. Islam MA, Riaz TA, Hossain MA, Lee I, Akter J, Shrestha S, Gyawali N, Pandey A, Chaizul S, Fualo V and Hahn JR: Controlled release of Ag^{+} ions to human cancer cells selectively neutralized with silver nanoparticles of different sizes produced by a green synthesis method. J Mol Struct 1294: 136384, 2023.
58. Lu L, Hu J and Xiong M: Chemical characterization, antioxidant, cytotoxicity, and anti-human breast cancer potentials of *Allium ampeloprasum* green-formulated silver nanoparticles by investigating the p53 and cell cycle G1, S, G2, and M phases. Arab J Chem 19: 10452025, 2026.
59. Putri GFT and Nurfatihah Z Z: Bax/Bcl-2 ratio as the golden marker of apoptosis: Molecular mechanisms and regulatory pathways. Int J Cell Biomed Sci 4: 309-317, 2025.
60. Xu J, Chen Y and Olopade OI: MYC and breast cancer. Genes Cancer 1: 629-640, 2010.
61. Montalto FI and De Amicis F: Cyclin D1 in cancer: A molecular connection for cell cycle control, adhesion and invasion in tumor and stroma. Cells 9: 2648, 2020.
62. Jana D, Sarkar DK, Ganguly S, Saha S, Sa G, Manna AK, Banerjee A and Mandal S: Role of cyclooxygenase 2 (COX-2) in prognosis of breast cancer. Indian J Surg Oncol 5: 59-65, 2014.
63. Hsu JL and Hung MC: The role of HER2, EGFR, and other receptor tyrosine kinases in breast cancer. Cancer Metastasis Rev 35: 575-588, 2016.
64. Dewi FRP, Wahyuningsih SPA, Sari APM, Alfiah UN, Lim V, Zubaidah U and Hayati A: Annonacin and squamocin conjugation with nanodiamond alters metastatic marker expression in breast cancer cell line. HAYATI J Biosci 31: 211-220, 2024.
65. Salado J, Insausti M, Lezama L, Gil de Muro I, Moros M, Pelaz B, Grazu V, de la Fuente JM and Rojo T: Functionalized Fe_3O4@Au superparamagnetic nanoparticles: In vitro bioactivity. Nanotechnology 23: 315102, 2012.
66. Cho TJ, MacCuspie RI, Gigault J, Gorham JM, Elliott JT and Hackley VA: Highly stable positively charged dendron-encapsulated gold nanoparticles. Langmuir 30: 3883-3893, 2014.
67. Aueviriyavit S, Phummiratch D and Maniratanachote R: Mechanistic study on the biological effects of silver and gold nanoparticles in Caco-2 cells-induction of the Nrf2/HO-1 pathway by high concentrations of silver nanoparticles. Toxicol Lett 224: 73-83, 2014.
68. Rahim S, Ali SA, Ahmed F, Imran M, Shah MR and Malik MI: Evaluation of morphology, aggregation pattern and size-dependent drug-loading efficiency of gold nanoparticles stabilised with poly (2-vinyl pyridine). J NanopartRes 19: 259, 2017.
69. Souza FR, Fornasier F, Carvalho AS, Silva BM, Lima MC and Pimentel AS: Polymer-coated gold nanoparticles and polymeric nanoparticles as nanocarrier of the BP100 antimicrobial peptide through a lung surfactant model. J Mol Liq 314: 113661, 2020.
70. Venditti I, Cartoni A, Cerra S, Fioravanti R, Salamone TA, Sciubba F, Tabocchini MA, Dini V, Battocchio C, Iucci G, *et al*: Hydrophilic gold nanoparticles as anti-PD-L1 antibody carriers: Synthesis and interface properties. Part Part Syst Charact 39: 2100282, 2022.
71. Poonaki E, Nickel AC, Shafiee Ardestani M, Rademacher L, Kaul M, Apartsin E, Meuth SG, Gorji A, Janiak C and Kahlert UD: CD133-functionalized gold nanoparticles as a carrier platform for telaglenastat (CB-839) against tumor stem cells. Int J Mol Sci 23: 5479, 2022.
72. Milán-Rois P, Rodriguez-Diaz C, Castellanos M and Somoza Á: Conjugation of nucleic acids and drugs to gold nanoparticles. In: Arechavala-Gomeza V and Garanto A (eds) Antisense RNA Design, Delivery, and Analysis. Methods in Molecular Biology. Vol. 2434. Humana, New York, NY, pp103-116, 2022.
73. Kong FY, Zhang JW, Li RF, Wang ZX, Wang WJ and Wang W: Unique roles of gold nanoparticles in drug delivery, targeting and imaging applications. Molecules 22: 1445, 2017.